Two high-pressure superconducting phases in pressurized optical semiconductor GaP

Nixian Qian[1,2], Chunhua Chen[1], Yonghui Zhou[1,2], Shuyang Wang[1], Liangyu Li[1,2], Ranran Zhang[1], Xiangde Zhu[1,2], Yifang Yuan[3], Xuliang Chen[1,2], Chao An[4], Ying Zhou[4], Min Zhang[4], Xiaoping Yang[1,2] and Zhaorong Yang[1,2,4,5]

Abstract
Pressure engineering in semiconductors leads to a variety of novel physical phenomena and has recently received considerable attention. Here, we report on pressure-induced superconductivity in III–V gallium phosphide (GaP), a commercially important semiconductor that exhibits excellent optical performance. We show that the emergence of superconductivity is accompanied by the concurrence of piezochromic transition and metallization and can be correlated to a structural transition from the cubic to orthorhombic phase. In line with the structural origin of superconductivity, the critical temperature T_c monotonically decreases with increasing pressure up to ~50 GPa. Moreover, the superconductivity could be preserved toward ambient pressure because of the irreversibility of the structural transition. Nevertheless, the superconducting transition displays evident broadening associated with the presence of amorphization in the depressurized sample. The synchronous evolution of the structural and electronic properties not only shows a vivid structure-property relationship but also could facilitate the exploration of novel functionalities by means of pressure treatment.

Introduction

As a highly representative III–V compound semiconductor, gallium phosphide (GaP) has attracted immense interest, which crystalizes in either zincblende or wurtzite structures at ambient pressure[1,2]. Zincblende GaP possesses extensive practical applications in the fields of light-emitting diodes, near-infrared optics, photonic crystals, and photocatalysis owing to its noncentrosymmetric crystal structure, large second-order nonlinearity, nonzero piezoelectric coefficient and high refractive index across the visible and near-infrared regime[3–7]. Nanostructured counterparts with various morphologies also display fascinating properties and have become promising materials for efficient second harmonic generation, ultrafast all-optical modulators, and integrated nonlinear photonics waveguides[8–11]. Moreover, nanostructured GaP can be further fabricated and applied in metasurface-based nanophotonics[12–15]. In contrast to the zincblende structure, which has an indirect bandgap of 2.26 eV, hexagonal wurtzite-type GaP nanowires host a direct bandgap and can be used as green light emitter candidates[1,16].

Pressure, as a thermodynamic variable, is an effective and powerful way to modulate the crystal lattice as well as electronic states, thereby documenting the structure-property relationship of materials[17–20]. Recently, pressure-tuned crystal structure and physical properties have been reported among various layered optoelectronic and photovoltaic semiconductors, such as MoS_2, ReS_2, and $SnSe$[21–24]. Due to the excellent optical functionalities of three-dimensional GaP semiconductors with wide bandgaps mentioned above, their structural and electronic properties under pressure have been thoroughly studied in the past decades. It is now widely accepted that

Correspondence: Yonghui Zhou (yhzhou@hmfl.ac.cn) or
Xiaoping Yang (xpyang@hmfl.ac.cn) or Zhaorong Yang (zryang@issp.ac.cn)
[1]Anhui Province Key Laboratory of Condensed Matter Physics at Extreme Conditions, High Magnetic Field Laboratory, HFIPS, Chinese Academy of Sciences, Hefei 230031, China
[2]Science Island Branch of Graduate School, University of Science and Technology of China, Hefei 230026, China
Full list of author information is available at the end of the article
These authors contributed equally: Nixian Qian, Chunhua Chen

GaP undergoes a cubic-to-orthorhombic transition (*F*-43*m* to *Cmcm*) at a pressure slightly above 20 GPa, concomitant with the simultaneous appearance of metallization[25–28]. Moreover, the decompressed sample is mainly amorphous, indicating the irreversibility of the structural transition[28–30]. Compared with the systematic investigation of structural evolution under pressure, the study of electrical transport is limited[28,31,32]. Apart from some electrical transport studies conducted above the liquid nitrogen temperature, the low-temperature electrical properties of GaP under pressure are yet unexplored to date.

Here, we investigated the structure-property relationship of bulk GaP crystals by combining optical micrographic, Raman spectroscopic, and electrical transport measurements under high pressure. We show that the cubic-orthorhombic phase transition not only leads to the occurrence of piezochromic transition and metallization but also gives rise to the emergence of superconductivity. In accordance with the irreversible structural transition, the evolution of electronic properties is also irreversible. The superconductivity can be retained toward ambient pressure and displays broadening features due to the presence of amorphization.

Materials and methods

Synthesis and characterization of GaP at ambient pressure

GaP single crystals were synthesized by the Czochralski method[33]. Room-temperature X-ray diffraction (XRD) patterns of single crystals were obtained with Cu K_α radiation ($\lambda = 1.5406$ Å) using a Rigaku X-ray diffractometer (Miniflex-600). The atomic proportion of the crystal was confirmed by energy dispersive X-ray spectroscopy (EDXS, Helios Nanolab 600i, FEI) via area-scanning mode.

Raman spectra, synchrotron X-ray diffraction, electrical transport, and *ac* magnetic susceptibility measurements under high pressure

High-pressure experimental details were similar to those in ref. [34]. The culet of the diamond was 300 μm. Raman spectra were recorded on bulk crystal GaP surfaces by using a Renishaw spectrometer with a pseudo backscattering configuration ($\lambda = 532$ nm). The laser power was kept below 2.5 mW to avoid sample damage and heating effects. The back-scattered signal was collected in an unpolarized geometry through a 20× objective and 1800 g/mm grating. A powder angle-dispersive synchrotron X-ray diffraction experiment was carried out using the beamline BL15U1 at the Shanghai Synchrotron Radiation Facility ($\lambda = 0.6199$ Å). Silicone oil was used as the pressure-transmitting medium (PTM). The *ac* magnetic susceptibility was measured using a magnetic inductance technique as reported previously[35]. The excitation current was 1 mA with a frequency of 1997 Hz.
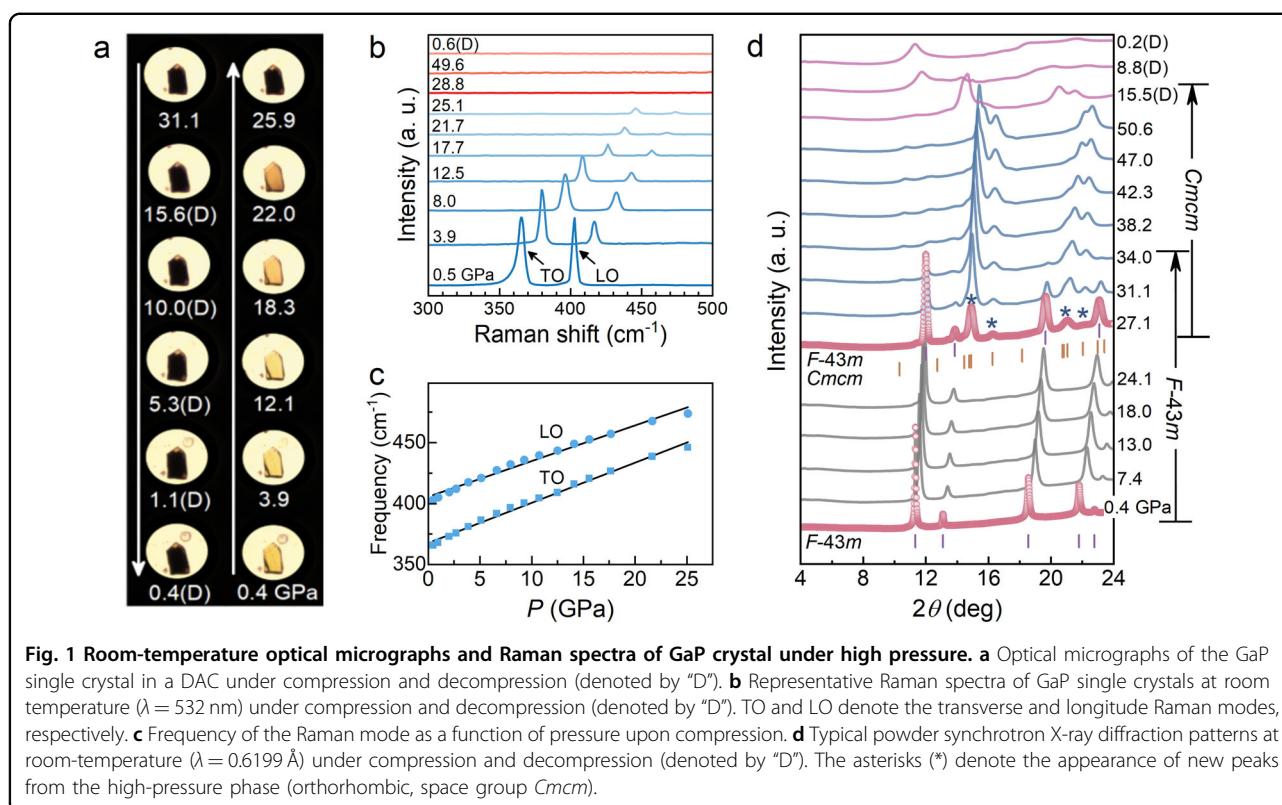
Systematic transport measurements with PTM NaCl were further performed in a four-probe configuration. The applied magnetic field was perpendicular to the surface of the flake. The pressure values for all of the above experiments were determined via the ruby fluorescence method at room temperature[36].

Results and discussion

The structural and physical properties of the GaP single crystal at ambient pressure were characterized via XRD, EDS, and Raman spectroscopic measurements, as shown in Fig. S1. Bulk GaP has a cubic structure (space group *F*-43m) and contains two atoms in a primitive cell. The as-grown GaP single crystal was yellowish, and its surface was oriented along (h00). The EDS measurement yielded a composition of $GaP_{0.97}$. Two Raman peaks were observed at 367 and 405 cm^{-1} from the room-temperature Raman spectrum in the range of 300–500 cm^{-1}, which could be assigned to the transverse optical (TO) and longitudinal optical (LO) modes, respectively[37]. All results indicate the good quality of our samples.

We first investigated the effect of pressure on the optical properties of GaP crystals at room temperature. As shown in Fig. 1a, the optical micrographs recorded at various pressures indicate that GaP changes from transparent yellowish to opaque black with increasing pressure above 22.0 GPa and remains opaque black upon further decompression from 31.1 to 0.4 GPa. This color change at approximately 22.0 GPa demonstrates a piezochromic transition with irreversibility after a compression-decompression cycle. This phenomenon is strongly correlated with the structural phase transition[25,26,38]. The relatively small color change of GaP below 22.0 GPa is compatible with the pressure variation of E_g of -14.9 meV GPa^{-1} extracted from the early high-pressure transmission experiments[39]. At 17 GPa, the indirect bandgap of ~2.0 eV is equal to 620 nm in the orange region (590 to 625 nm) according to the formula $E_g = 1240/\lambda$ (eV)[39].

To further investigate the pressure evolution of the lattice vibrational property of the GaP crystal, we performed Raman spectroscopic measurements at room temperature. Figure 1b displays the representative Raman spectra of GaP under high pressure. At 0.5 GPa, there exists two Raman modes, TO and LO, which are similar to those at ambient pressure (see Fig. S1d). With increasing pressure, both the TO and LO modes are continuously shifted toward higher wavenumbers and show a progressive reduction in intensity. Then, these two modes disappear above 25.1 GPa, where the Raman spectrum remains featureless under decompression from 49.6 to 0.6 GPa. Moreover, the high-pressure X-ray diffraction experiment shows a cubic-to-orthorhombic

Fig. 1 Room-temperature optical micrographs and Raman spectra of GaP crystal under high pressure. a Optical micrographs of the GaP single crystal in a DAC under compression and decompression (denoted by "D"). **b** Representative Raman spectra of GaP single crystals at room temperature ($\lambda = 532$ nm) under compression and decompression (denoted by "D"). TO and LO denote the transverse and longitude Raman modes, respectively. **c** Frequency of the Raman mode as a function of pressure upon compression. **d** Typical powder synchrotron X-ray diffraction patterns at room-temperature ($\lambda = 0.6199$ Å) under compression and decompression (denoted by "D"). The asterisks (*) denote the appearance of new peaks from the high-pressure phase (orthorhombic, space group *Cmcm*).
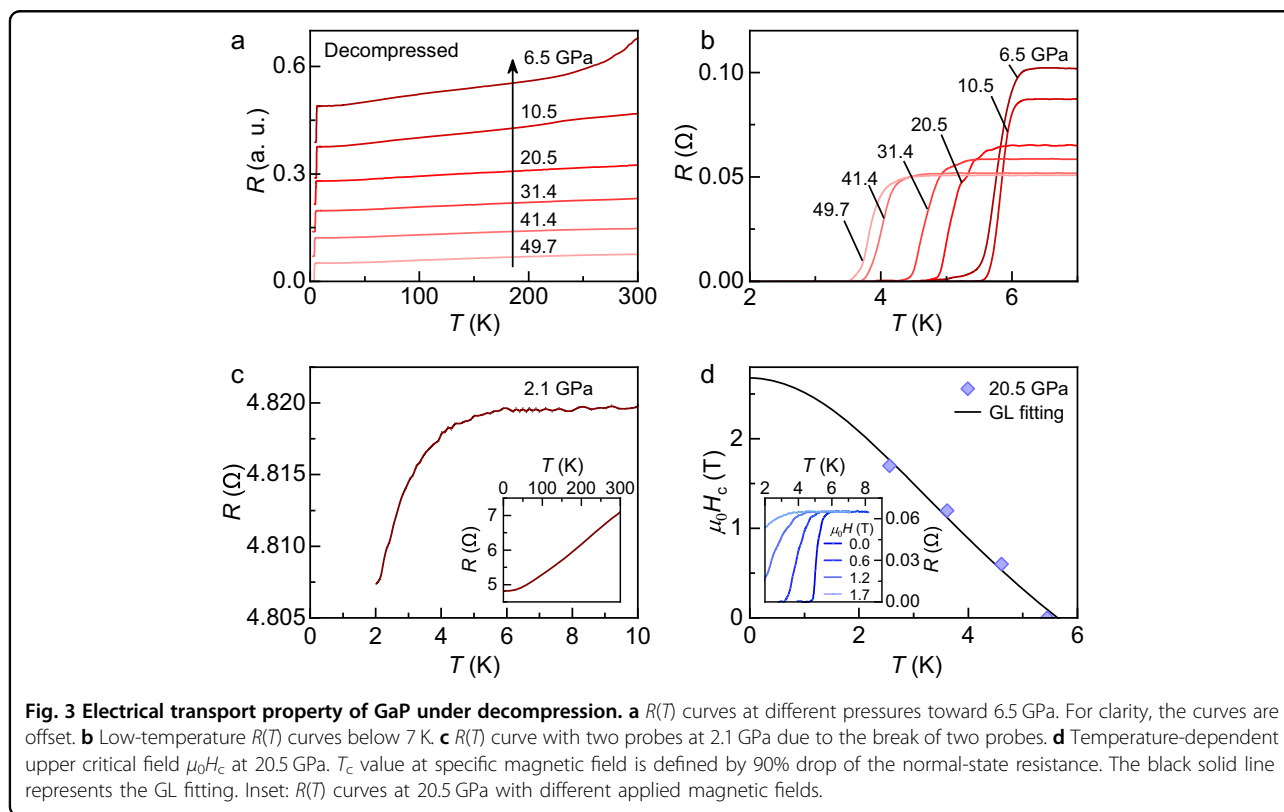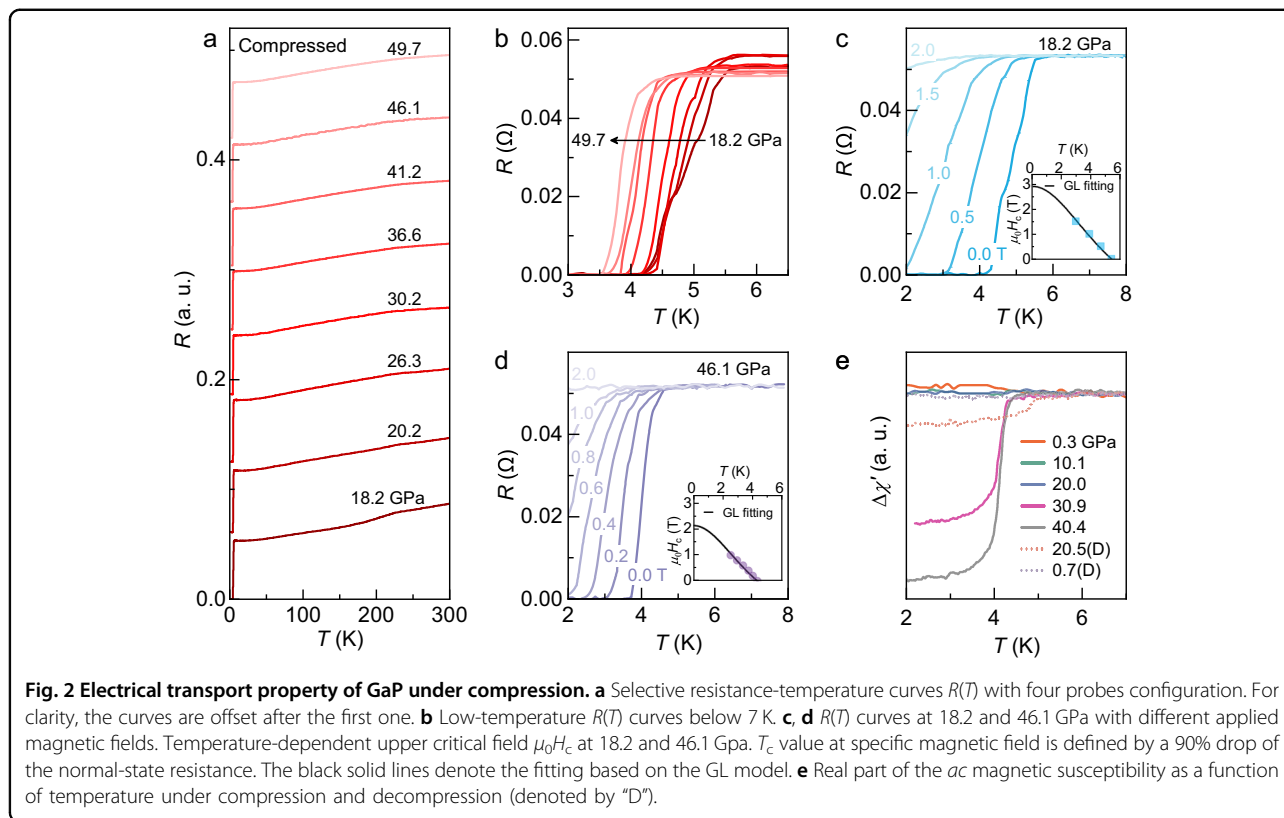
transition at 27.1 GPa and mainly amorphous features upon decompression to 0.2 GPa, indicating the irreversibility of the structural transition, as shown in Fig. 1d. This is consistent with the early experimental literatures[25–27]. The extracted lattice parameters and volume as a function of pressure are shown in Fig. S2. Therefore, the disappearance of Raman modes upon compression could be related to the structural phase transition. Additionally, the preservation of featureless Raman could be due to the presence of amorphization in the depressurized sample[28,30]. Fig. 1c shows the pressure-dependent Raman modes. For the TO and LO modes, the slopes extracted by linear fitting are 3.3 and 2.9 cm^{-1} GPa^{-1}, respectively.

To explore the conductivity change of the sample, we performed a high-pressure transport experiment. Figure 2a shows representative temperature-dependent resistance $R(T)$ curves. Due to the upper limit of the experimental setup ($<10^7$ Ω), the room-temperature resistance of the sample could only be detected with a gradual approach to 18.2 GPa. Clearly, at 18.2 GPa, GaP displays metallic behavior over the entire temperature range. The appearance of metallization is accompanied by a resistance decrease of several orders of magnitude, similar to the results of refs. [31,32]. Metallic conductivity and zero resistance are simultaneously observed, signaling the concurrence of metallization and the superconducting transition in pressurized GaP. Further high-pressure *ac*

magnetic susceptibility measurements show the Meissner effect above 20 GPa, indicating the bulk nature of superconductivity (see Fig. 2e). The zero-resistance state retains under compression to 49.7 GPa, as shown in Fig. 2b. The critical magnetic field of superconducting GaP is measured by varying the external magnetic field at 18.2 and 46.1 GPa. The superconducting transition is gradually shifted toward lower temperatures and is nearly suppressed above 2.0 T (see Fig. 2c, d). The temperature-magnetic field phase diagram is plotted in Fig. 2e. By fitting the data to the GL model, the upper critical field $\mu_0 H_c(0)$ is 2.9 and 2.15 T at 18.2 and 46.1 GPa, respectively. These are much lower than the corresponding Pauli limiting field of $\mu_0 H_P(0) = 1.84 T_c$[40].

Based on the irreversibility of the structural phase transition and the presence of amorphization in the depressurized GaP, we further investigated the electrical transport behavior when the pressure was gradually released from 49.7 GPa, as shown in Fig. 3. GaP does not recover to its original insulating state with decreasing pressure to 2.1 GPa. The superconducting transition width appears to be inert to pressures above 6.5 GPa but becomes much larger at 6.5 GPa, as reflected by the tail in the $R(T)$ curve before reaching the zero-resistance state. Since the two probes were suddenly broken at 2.1 GPa, we did not observe zero resistance upon cooling to 2 K. Nevertheless, the metallic conductivity is maintained at this pressure, as shown in the inset

Fig. 2 Electrical transport property of GaP under compression. a Selective resistance-temperature curves $R(T)$ with four probes configuration. For clarity, the curves are offset after the first one. **b** Low-temperature $R(T)$ curves below 7 K. **c, d** $R(T)$ curves at 18.2 and 46.1 GPa with different applied magnetic fields. Temperature-dependent upper critical field $\mu_0 H_c$ at 18.2 and 46.1 Gpa. T_c value at specific magnetic field is defined by a 90% drop of the normal-state resistance. The black solid lines denote the fitting based on the GL model. **e** Real part of the *ac* magnetic susceptibility as a function of temperature under compression and decompression (denoted by "D").

Fig. 3 Electrical transport property of GaP under decompression. a $R(T)$ curves at different pressures toward 6.5 GPa. For clarity, the curves are offset. **b** Low-temperature $R(T)$ curves below 7 K. **c** $R(T)$ curve with two probes at 2.1 GPa due to the break of two probes. **d** Temperature-dependent upper critical field $\mu_0 H_c$ at 20.5 GPa. T_c value at specific magnetic field is defined by 90% drop of the normal-state resistance. The black solid line represents the GL fitting. Inset: $R(T)$ curves at 20.5 GPa with different applied magnetic fields.

of Fig. 3c. We measured the critical magnetic field of superconducting GaP at 20.5 GPa. The upper critical field $\mu_0H_c(0)$ is 2.68 T, which is comparable to that of 18.2 GPa under compression (Fig. 2c). This result demonstrates that the superconductivity is preserved toward ambient pressure, indicating the irreversibility of the electrical transport properties after a compression-decompression cycle. According to the XRD results and early literature[30], this result also indicates the presence of superconductivity embedded in the amorphous phase.

Based on these transport results and the pressure evolution of the crystal structure[28,30], we constructed a comprehensive phase diagram to elucidate the structure-property relationship in pressurized cubic GaP, as depicted in Fig. 4. This clearly demonstrates the structural origin of the unusual evolution of electrical properties. First, since the structural phase transition from the LP to HP phase leads to a unit-cell volume contraction of ~15.5% at a critical pressure P_c of ~18 GPa[17], such a large volume variation can account for the immediate appearance of both metallization and superconductivity. Simultaneously, a piezochromic transition and

featureless Raman spectra were observed around the structural phase transition. Note that the discrepancy in the critical transition pressure in the different experiments could be attributed to the pressure distribution due to the difference in the pressure medium[41]. Although the HP orthorhombic structure with the D_{2h} point group could host Raman-active modes according to the group theoretical analysis, no Raman mode was observed in the high-pressure phase due to the metallic conductivity[42]. Second, a decrease in T_c with increasing pressure in the HP phase, namely, a negative pressure effect on the superconductivity, could be easily accounted for within Bardeen–Cooper–Schrieffer (BCS) theory, which is based on an electron-phonon pairing interaction[43,44]. We further calculated the electronic band structures and density of states (DOSs) at the Fermi level of the HP phase, as shown in Fig. S3. Notably, the overall band evolution remains relatively stable, while the DOS peak value decreases within the range of 0.25 eV. Thus, the decreased DOS along with lattice stiffening could be responsible for the observed decrease in T_c with increasing pressure in HP superconducting GaP within BCS theory. For the amorphous
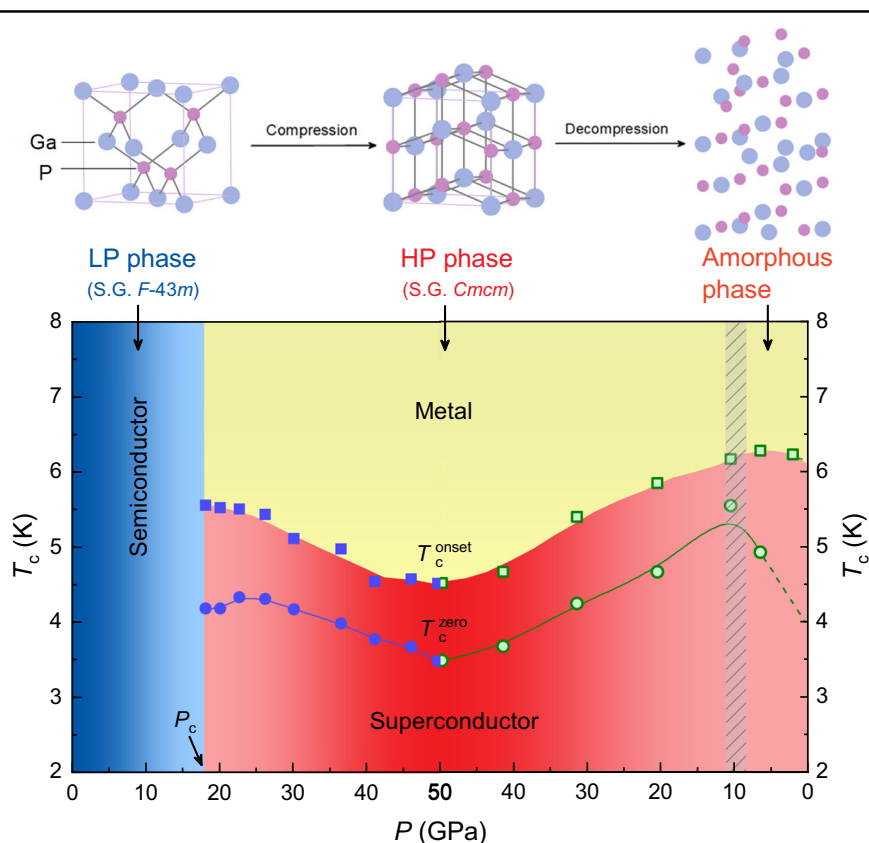

Fig. 4 Relationship between the structural and electronic properties in pressurized GaP bulk. The onset and zero-resistance transition temperature T_c's are extracted from the R(T) curves. The blue and green symbols denote the data from the compression and decompression processes, respectively. The dashed lines below 6.5 GPa are guides to the eye. The colored areas indicate the different electronic state along with the different crystal structures, i.e., pristine low-pressure (LP) phase (cubic, S.G. F-43m, Z = 4), high-pressure (HP) phase (orthorhombic, S.G. Cmcm, Z = 2), and amorphous phase. The dashed gray area is correlated to the transformation between the HP and amorphous phase under decompression.

phase developed during the decompression process, however, the T_c evolution versus pressure shows a positive pressure effect. Considering the formation of a mainly amorphous structure during decompression, this is likely correlated with the metastable amorphous structure with disorder. Third, the irreversibility of the structural transition after a compression-decompression cycle is consistently reflected by the preserved metallic conductivity and the unrecovered Raman modes. Lastly, although the GaP decompressed from 49.7 GPa is reminiscent of as-grown amorphous GaP[45], the decompressed amorphous GaP exhibited metallic conductivity, as shown in Fig. 3c. This result indicates that different amorphous states of GaP with fine local structure features could host different physical properties in nature. Apart from the same superconducting phenomenon in both the HP orthorhombic phase of GaP and its derivative $ZnGeP_2$[34], they have some differences as follows: (1) GaP crystalizes in a cubic structure at ambient pressure. $ZnGeP_2$ hosts a cubic phase as its first HP phase with cation disorder. (2) Similar amorphous behavior during decompression was observed for both GaP and $ZnGeP_2$; this could be attributed to the connection with the pressure dependence of kinetic barriers for the phase transitions by using a configuration-coordinate model.[29] However, the starting phases of amorphization are different, i.e., orthorhombic in GaP versus cubic in $ZnGeP_2$. Therefore, the same amorphous superconductivity in GaP and $ZnGeP_2$ is likely caused by their different parent lattices.

Conclusion

In summary, we have investigated the relationship between the structural, optical, and electrical properties of bulk GaP single crystals at high pressures by combining Raman scattering, piezochromism, synchrotron X-ray diffraction, electrical transport, and *ac* magnetic susceptibility experiments. We show that pressure-engineered electronic properties are effectively correlated with the structural and optical evolutions. During compression, metallization and superconductivity simultaneously appear, which is accompanied by a piezochromic transition and attributed to the appearance of a structural transition from the cubic to orthorhombic phase. Upon further decompression, the superconductivity is preserved toward ambient pressure, consistent with the irreversibility of the cubic-orthorhombic phase transition and the presence of an amorphous phase in the depressurized sample. The newly observed two high-pressure superconducting phases, as well as the irreversible evolution of the structural and electrical properties provide a comprehensive understanding of the physical properties of semiconductor GaP under pressure.

Author details
[1]Anhui Province Key Laboratory of Condensed Matter Physics at Extreme Conditions, High Magnetic Field Laboratory, HFIPS, Chinese Academy of Sciences, Hefei 230031, China. [2]Science Island Branch of Graduate School, University of Science and Technology of China, Hefei 230026, China. [3]Key Laboratory of Material Physics, Ministry of Education, School of Physics and Microelectronics, Zhengzhou University, Zhengzhou 450001, China. [4]Institutes of Physical Science and Information Technology, Anhui University, Hefei 230601, China. [5]Collaborative Innovation Center of Advanced Microstructures, Nanjing University, Nanjing 210093, China

Author contributions
Y-H.Z. and Z.Y. conceived the study and explained the experimental results. N.Q. synthesized the single crystal. N.Q., C.C., S.W., R.Z., X.Z., Y.Y., X.C., C.A., Y.Z. and M.Z. measured the physical properties of the sample. L.L. and X.Y. performed the theoretical calculations. N.Q., Y-H.Z. and Z.Y. analyzed the data and wrote the paper and Supplementary Information. All authors were involved in the discussion of the results and approved the final version of the manuscript.

Conflict of interest
The authors declare no competing interests.

Publisher's note
Springer Nature remains neutral with regard to jurisdictional claims in published maps and institutional affiliations.

References
1. Assali, S. et al. Direct band gap wurtzite gallium phosphide nanowires. *Nano Lett.* **13**, 1559 (2013).
2. Tilmann, B. et al. Nanostructured amorphous gallium phosphide on silica for nonlinear and ultrafast nanophotonics. *Nanoscale Horiz.* **5**, 1500 (2020).
3. Aspnes, D. E. & Studna, A. A. Dielectric functions and optical parameters of Si, Ge, GaP, GaAs, GaSb, InP, InAs, and InSb from 1.5 to 6.0 eV. *Phys. Rev. B* **27**, 985 (1983).
4. Lessio, M. & Carter, E. A. What is the role of pyridinium in pyridine-catalyzed CO_2 reduction on p-GaP photocathodes? *J. Am. Chem. Soc.* **137**, 13248 (2015).
5. Lorenz, M. R., Pettit, G. D. & Taylor, R. C. Band gap of gallium phosphide from 0 to 900°K and light emission from diodes at high temperatures. *Phys. Rev.* **171**, 876 (1968).
6. Wilson, D. J. et al. Integrated gallium phosphide nonlinear photonics. *Nat. Photonics* **14**, 57 (2020).
7. Rutkauskas, M., Srivastava, A. & Reid, D. T. Supercontinuum generation in orientation-patterned gallium phosphide. *Optica* **7**, 172 (2020).
8. Sanatinia, R., Anand, S. & Swillo, M. Modal engineering of second-harmonic generation in single GaP nanopillars. *Nano Lett.* **14**, 5376 (2014).
9. Cambiasso, J. et al. Bridging the gap between dielectric nanophotonics and the visible regime with effectively lossless gallium phosphide antennas. *Nano Lett.* **17**, 1219 (2017).

10. Grinblat, G. et al. Efficient ultrafast all-optical modulation in a nonlinear crystalline gallium phosphide nanodisk at the anapole excitation. *Sci. Adv.* **6**, eabb3123 (2020).

11. Bolshakov, A. D. et al. Single GaP nanowire nonlinear characterization with the aid of an optical trap. *Nanoscale* **14**, 993 (2022).

12. Karawdeniya, B. I. et al. Surface functionalization and texturing of optical metasurfaces for sensing applications. *Chem. Rev.* **122**, 14990 (2022).

13. Melli, M. et al. Gallium phosphide optical metasurfaces for visible light applications. *Sci. Rep.* **10**, 20694 (2020).

14. Anthur, A. P. et al. Continuous wave second harmonic generation enabled by quasi-bound-states in the continuum on gallium phosphide metasurfaces. *Nano Lett.* **20**, 8745 (2020).

15. Shcherbakov, M. R. et al. Generation of even and odd high harmonics in resonant metasurfaces using single and multiple ultra-intense laser pulses. *Nat. Commun.* **12**, 4185 (2021).

16. Dasgupta, N. P. et al. 25th anniversary article: semiconductor nanowires - synthesis, characterization, and applications. *Adv. Mater.* **26**, 2137 (2014).

17. Ackland, G. J. High-pressure phases of group IV and III-V semiconductors. *Rep. Prog. Phys.* **64**, 483 (2001).

18. Mujica, A., Rubio, A., Muñoz, A. & Needs, R. J. High-pressure phases of group-IV, III–V, and II–VI compounds. *Rev. Mod. Phys.* **75**, 863 (2003).

19. Li, Q. et al. Pressure-induced superconductivity in HgTe single-crystal film. *Adv. Sci.* **9**, 2200590 (2022).

20. Liang, Y. et al. New metallic ordered phase of perovskite $CsPbI_3$ under pressure. *Adv. Sci.* **6**, 1900399 (2019).

21. Chi, Z. H. et al. Superconductivity in pristine 2Ha-MoS₂ at ultrahigh pressure. *Phys. Rev. Lett.* **120**, 037002 (2018).

22. Zhou, D. W. et al. Pressure-induced metallization and superconducting phase in ReS2. *npj Quantum Mater.* **2**, 19 (2017).

23. Chen, X. L. et al. Topological Dirac line nodes and superconductivity coexist in SnSe at high pressure. *Phys. Rev. B* **96**, 165123 (2017).

24. Liu, G. et al. Pressure-induced bandgap optimization in lead-based perovskites with prolonged carrier lifetime and ambient retainability. *Adv. Funct. Mater.* **27**, 1604208 (2016).

25. Nelmes, R. J., McMahon, M. I. & Belmonte, S. A. Nonexistence of the diatomic tin structure. *Phys. Rev. Lett.* **79**, 3668 (1997).

26. Ono, S. & Kikegawa, T. Determination of the phase boundary of GaP using in situ high pressure and high-temperature X-ray diffraction. *High. Press. Res.* **37**, 28 (2017).

27. Baublitz, M. & Ruoff, A. L. Diffraction studies of the high pressure phases of GaAs and GaP. *J. Appl. Phys.* **53**, 6179 (1982).

28. Dai, L. et al. Characterization of metallization and amorphization for GaP under different hydrostatic environments in diamond anvil cell up to 40.0 GPa. *Rev. Sci. Instrum.* **90**, 066103 (2019).

29. Tsuji, K., Katayama, Y., Yamamoto, Y., Kanda, H. & Nosaka, H. Amorphization from quenched high-pressure phase in tetrahedrally bonded materials. *J. Phys. Chem. Solid.* **56**, 559 (1995).

30. Tsuji, K., Katayama, Y., Kanda, H. & Nosaka, H. Amorphization from the quenched high-pressure phase in GaAs and GaP. *J. Non Cryst. Solids* **518**, 205 (1996).

31. Li, Y. Q. et al. Electrical transport properties of gallium phosphide under high pressure. *Phys. Status Solidi B* **257**, 1900470 (2019).

32. Liu, H. et al. Pressure effects on the metallization and dielectric properties of GaP. *Phys. Chem. Chem. Phys.* **23**, 26829 (2021).

33. Kokubun, Y., Washizuka, S., Ushizawa, J., Watanabe, M. & Fukuda, T. Properties of high quality GaP single crystals grown by computer controlled liquid encapsulated Czochralski technique. *Appl. Phys. Lett.* **41**, 841 (1982).

34. Yuan, Y. F. et al. Pressure induced superconductivity in nonlinear optical crystal ZnGeP₂ and its capture at ambient pressure. *Mater. Today Phys.* **25**, 100707 (2022).

35. Pan, X. C. et al. Pressure-driven dome-shaped superconductivity and electronic structural evolution in tungsten ditelluride. *Nat. Commun.* **6**, 7805 (2015).

36. Mao, H. K., Xu, J. & Bell, P. M. Calibration of the ruby pressure gauge to 800 kbar under quasi-hydrostatic conditions. *J. Geophys. Res.* **91**, 4673 (1986).

37. Hobden, M. V. & Russell, J. P. The Raman spectrum of gallium phosphide. *Phys. Lett.* **13**, 39 (1964).

38. Aquilanti, G. et al. High-pressure phase of GaP: structure and chemical ordering. *Phys. Rev. B* **76**, 064103 (2007).

39. Jauberthie-Carillon, C. & Guillemin, C. Dependence of the indirect energy gap of GaP on quasihydrostatic pressure and phase transition. *J. Phys. Condens. Matter* **1**, 6807 (1989).

40. Ginzburg, V. L. & Landau, L. D. *Zh. Eksp. Teor. Fiz.* **20**, 1064 (1950).

41. Klotz, S., Chervin, J. C., Munsch, P. & Le Marchand, G. Hydrostatic limits of 11 pressure transmitting media. *J. Phys. D Appl. Phys.* **42**, 075413 (2009).

42. Goncharov, A. F. & Struzhkin, V. V. Raman spectroscopy of metals, high-temperature superconductors and related materials under high pressure. *J. Raman Spectrosc.* **34**, 532 (2003).

43. Schilling, J. S. & Hamlin, J. J. Recent studies in superconductivity at extreme pressures. *J. Phys.: Conf. Ser.* **121**, 052006 (2008).

44. Hamlin, J. J. Superconductivity in the metallic elements at high pressures. *Physica C.* **514**, 59 (2015).

45. Itic, J. P., Polian, A. & Jauberthie-Carillon, C. High-pressure phase transition in gallium phosphide: An x-ray-absorption spectroscopy study. *Phys. Rev. B* **40**, 9709 (1989).